High-definition direct-print of metallic microdots with optical vortex induced forward transfer

Rong Wei ⓘ ; Haruki Kawaguchi ⓘ ; Kaito Sato ⓘ ; Sayaka Kai ⓘ ; Keisaku Yamane ⓘ ; Ryuji Morita ⓘ ;
Ken-ichi Yuyama ⓘ ; Satoyuki Kawano; Katsuhiko Miyamoto ⓘ ; Nobuyuki Aoki ⓘ ; Takashige Omatsu ✉ ⓘ

Check for updates

CHORUS

View Online

Export Citation
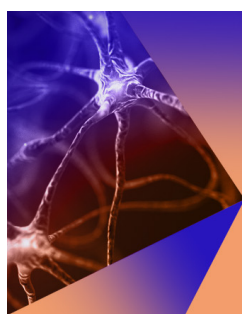
APL Photonics

Special Topic:
Photonics in Biomedicine

Submit Today

AIP Publishing

AIP Publishing

High-definition direct-print of metallic microdots with optical vortex induced forward transfer

View Online   Export Citation   CrossMark

Rong Wei,[1]   Haruki Kawaguchi,[1]   Kaito Sato,[1]   Sayaka Kai,[1]   Keisaku Yamane,[2]
Ryuji Morita,[2]   Ken-ichi Yuyama,[3]   Satoyuki Kawano,[4]   Katsuhiko Miyamoto,[1,5]
Nobuyuki Aoki,[1,5]   and Takashige Omatsu[1,5,a]

AFFILIATIONS

[1] Graduate School of Engineering, Chiba University, 1-33 Yayoi-cho, Inage-ku, Chiba 263-8522, Japan
[2] Department of Applied Physics, Hokkaido University, Kita-13, Nishi-8, Kita-ku, Sapporo 060-8628, Japan
[3] Department of Chemistry, Osaka Metropolitan University, 3-3-138 Sugimoto Sumiyoshi-ku, Osaka 558-8585, Japan
[4] Graduate School of Engineering Science, Osaka University, 1-3 Machikaneyama, Toyonaka, Osaka 560-8531, Japan
[5] Molecular Chirality Research Center, Chiba University, 1-33 Yayoi-cho, Inage-ku, Chiba 263-8522, Japan

[a] Author to whom correspondence should be addressed: omatsu@faculty.chiba-u.jp

ABSTRACT

We demonstrate high-definition, direct-printing of micron-scale metallic dots, comprised of close-packed gold nanoparticles, by utilizing the optical vortex laser-induced forward transfer technique. We observe that the spin angular momentum of the optical vortex, associated with circular polarization, assists in the close-packing of the gold nanoparticles within the printed dots. The printed dots exhibit excellent electrical conductivity without any additional sintering processes. This technique of applying optical vortex laser-induced forward transfer to metallic dots is an innovative approach to metal printing, which does not require additional sintering. It also serves to highlight new insights into light–matter interactions.

I. INTRODUCTION

Nozzle-based ink-jet printing[1] is a well-established technology utilized for a non-contact deposition of materials. As a technique, it avoids many of the difficulties associated with other processes such as electron/ion-beam lithography and chemical synthesis,[2–4] and it has been widely applied across numerous fields, including printed electronics,[5–8] photonics,[9,10] and biomedical applications.[11,12] However, despite its broad applicability, it is not a particularly effective technique for high spatial resolution (the minimum printed dot diameter is typically measured to be 10–20 μm even for low viscosity materials)[13] deposition of highly viscous or very dense materials, owing to nozzle clogging effects.[14] In addition, additional sintering steps must be used in conjunction with nozzle-based ink-jet printing in order to produce devices for printed electronics. Laser-induced forward transfer (LIFT)[15–18] is a technique, which enables the direct deposition of materials with irradiation of a laser pulse, and it has

been widely studied as an alternative printing approach to ink-jet printing. It enables the selective transfer of a wide range of materials (herein referred to as donors), such as solids,[19,20] liquids,[21,22] and even high viscosity pastes,[23–25] onto a receiver substrate. However, conventional LIFT, implemented with the use of a light field possessing a planar wavefront, still struggles to directly print highly viscous or dense materials onto substrates with high spatial resolution and at millimeter-scale working distances.

An optical vortex[26,27] possesses a ring-shaped spatial profile and an orbital angular momentum (OAM) (characterized by an integer ℓ, termed the topological charge), of which both originate from its helical wavefront with an on-axis phase-singularity. Vortex laser beams have become a prominent field of research due to their broad range of applications across fundamental sciences and advanced technologies, including nano/micrometer-scale optical trapping and manipulation,[28] optical/quantum OAM multiplexing communications,[29–31] and super-resolution microscopes, which

20 April 2024 13:25:05

enable spatial resolution beyond the diffraction limit.[32] The dichroism between molecular enantiomers and optical vortices, which manifests as strong electric quadrupole fields generated in unique nanoparticle aggregates, has been theoretically and experimentally investigated.[33,34] Prior research has also revealed that the unique interaction between optical vortices and irradiated materials can be utilized as an innovative material processing technique. Here, the OAM of the optical vortex twists the irradiated materials, such as metal,[35,36] silicon,[37] and even photopolymers,[38,39] to produce helical structures, with the help of spin angular momentum (SAM, $s = \pm 1$) of the circular polarization[40] of the beam.

Recently, we and our co-workers have demonstrated a new LIFT technology utilizing an optical vortex laser pulse that had a helical wavefront (as opposed to the use of a conventional Gaussian beam with a planar wavefront). In this technique [herein referred to as optical vortex laser-induced forward transfer (OV-LIFT)[41]], the OAM of the optical vortex pulse is transferred to the irradiated donor material, twisting it, and under the right conditions, results in the ejection of a spinning, picoliter (pl)-scale, single donor droplet with a perfectly straight flight path, somewhat akin to a rifling bullet. This enabled the direct print of microdots of highly viscous materials (>1 Pa s), with high spatial resolution and a very long flight (working) distance. In addition, OV-LIFT enables microstructuring of nanoparticles within the donor droplet and can be used for the fabrication of exotic, multi-layered colloidal crystals that have structural color and are formed of hexagonally close-packed nanoparticles.[42]

In this paper, we demonstrate the two-dimensional direct-printing of well-aligned, perfectly circular microdots, formed of close-packed Au nanoparticles, with a diameter of less than 20 μm (minimum printed dot diameter is measured to be 9 μm) beyond the limitation of conventional nozzle-based ink-jet printing and a positioning error of <7 μm [this error was dominated by the positional accuracy (5 μm) of the piezo-actuator used in this work], by employing the OV-LIFT technique. We further observe that the as-printed dots exhibit excellent metallic properties, such as high electrical conductivity, without any additional sintering processes. Surprisingly, the SAM reinforces/weakens the close packing and sintering effects

of the Au nanoparticles, and it also significantly improves/worsens the positional accuracy of the printed dots. We believe that the OV-LIFT technique offers a new, time- and cost-saving approach for the development of next-generation printed electronic devices.

II. METHOD

The donor material used in this work was a gold nano-ink, comprised of high-density gold nanoparticles (average diameter: ~130 nm, standard deviation: 70 nm, particle density: ~10^{13} cm^{-3}) suspended in a water/glycol mix, and had a considerably high viscosity of ~10 mPa s. This donor material was dropped onto a glass substrate to form a film with a thickness of ~40 μm. The donor film had a relatively high optical density of 0.75 at 532 nm.

Figure 1(a) shows a schematic diagram of the experimental setup. A Q-switched nanosecond green laser (wavelength: 532 nm, pulse duration: ~1.8 ns) was used, and its output was converted to a first-order optical vortex with $\ell = 1$, through the use of a spiral phase plate (SPP). The optical vortex beam was loosely focused to an annular spot (with a diameter of 35 μm) onto the donor film using a spherical lens (NA 0.05). Figure 1(b) shows the spatial intensity profile of the irradiated optical vortex at a focal plane. The optical vortex exhibited an annular spatial form with good symmetry. The polarization state of the irradiating optical vortex beam was controlled using a quarter-wave plate (QWP). The ejection of a single microdroplet of donor material was achieved at a laser pulse energy of 2.3 μJ.

The ejected microdroplet was propelled and subsequently printed onto a glass substrate receiver that was placed ~0.5 mm away from the donor film. The temporal evolution of the donor microdroplet and its ejection was observed and captured using an ultrahigh-speed camera with a frame rate of 200 ns per frame (5 Mfps). Selective printing of patterns of microdroplets was achieved by mounting the receiver substrate to piezo-actuators (which had a positional accuracy of ~5 μm) and translating the receiver substrate relative to the donor film and irradiating vortex beam.
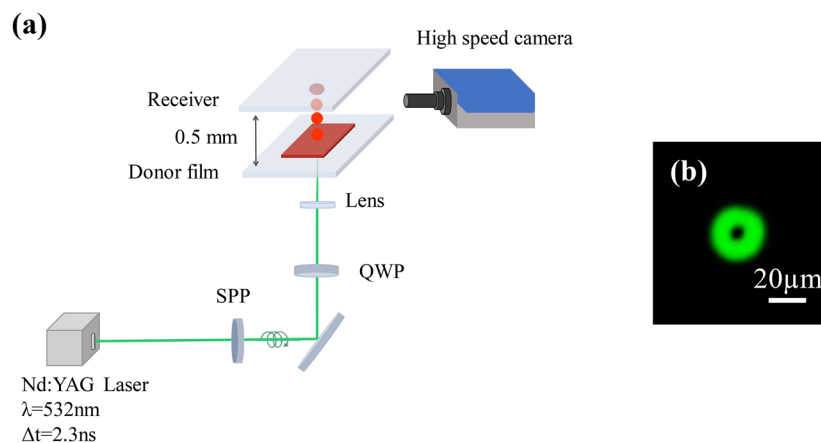
FIG. 1. (a) Schematic diagram of the experimental setup. (b) Spatial intensity form of the focused optical vortex beam captured using a CCD camera.

III. EXPERIMENTS

It was observed that a micrometer-scale jet of donor material was produced ~10 μs after irradiation of the donor material by the vortex beam. The region of the donor material illuminated by the vortex beam formed a blister, from which a jet of donor material was projected from the region of the material spatially correlated with the dark central region of the incident vortex beam. A single microdroplet (diameter: ~25 μm) was ejected from the tip of the jet due to the Plateau–Rayleigh instability [Fig. 2(a)]. The ejection of a single microdroplet only occurred for optical vortex pulse energies in the range 2.0–2.5 μJ. When the energy was lower than this level, droplets were never ejected from the material jet. At higher energy levels, multiple droplets were released from the jet.

In this work, the distance between the donor film and the receiver substrate was fixed at 0.5 mm. The ejected microdroplets impacted on the receiver substrate to form uniform,

circular dots of the donor material (diameter: <50 μm), which were comprised of close-packed gold nanoparticles [Fig. 2(b)]. Note that the droplet was mostly cooled via not thermal radiation during the flight but thermal conduction onto the receiver substrate.

Optical vortices with $J = 2$ ($\ell = 1$, $s = 1$) enabled the direct print of perfectly circular dots without any undesired debris, as evidenced by Bessel-function-like, multiple-ring-shaped high spatial frequency components with a period of ~0.04 cycle/μm (corresponding to the reciprocal of the radius of the printed dot) and without noise [Fig. 2(i)]. Surprisingly, the as-printed dots were also sintered [the nanoparticles were aggregated, as shown in Fig. 2(c)] and exhibited excellent electrical conductivity (10^{-7} Ω m measured by the Van der Pauw method). The height and surface roughness of the printed dots were measured using atomic force microscopy and found to be ~600 and ~22 nm, respectively. The results demonstrate that optical vortex beams with non-zero total angular momentum (TAM)
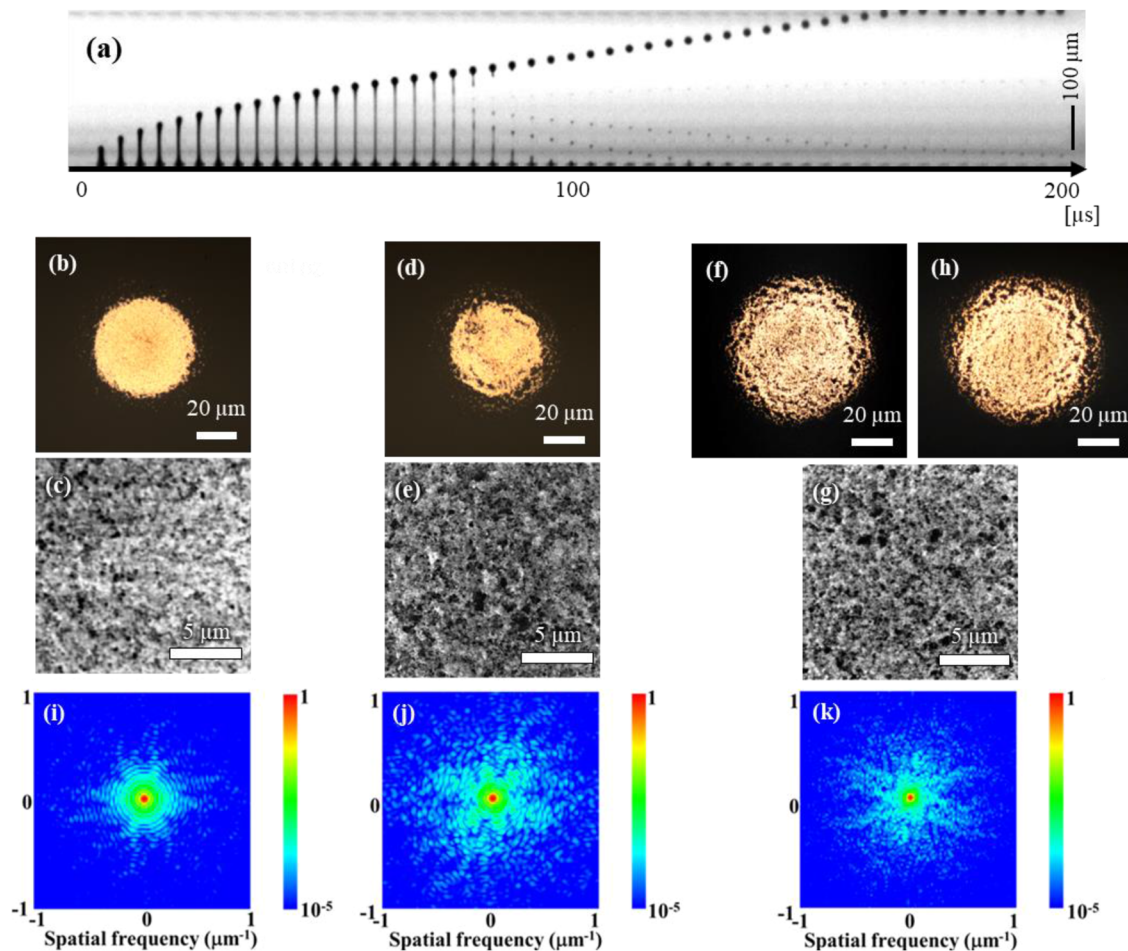
FIG. 2. (a) Time-lapse of the evolution of the droplet ejection from irradiation by an optical vortex pulse. Optical and SEM images of the printed dots fabricated by irradiation by an optical vortex with (b) and (c) $J = 2$ and (d) and (e) $J = 0$, and (f)–(h) a Gaussian beam [(h) circularly polarized Gaussian beam]. In the printed dots using an optical vortex with $J = 0$ and a Gaussian beam, close-packing and sintering of the gold nanoparticles were not observed. (i)–(k) Two-dimensional Fourier spectra of optical images [(b), (d), and (f)] of the printed dots. Printed dot with OV-LIFT exhibits a Bessel-function-like multiple ring-shaped profile with a period of ~0.04 cycle/μm.

can be used for the close-packing and sintering effects of the gold nanoparticles within OV-LIFT-printed dots.

Intriguingly, the SAM could be tailored to either reinforce or counteract the close-packing and sintering characteristic of the nanoparticles in the printed dots [Figs. 2(e)–2(g)]. Optical vortex beams with $J = 0$ ($\ell = 1$, $s = -1$) and circularly polarized Gaussian beams without OAM and even with SAM [$J = 1$ ($\ell = 0$, $s = 1$)] are unable to produce uniform dots and, instead, only produce non-uniform dots with undesired satellite debris at all pulse energy levels [Figs. 2(d)–2(f)]. In these cases, the diameter, height, and surface roughness of printed dots were typically measured to be 60–80 μm, ~300 nm, and ~35 nm, respectively. In fact, the printed dots with optical vortex ($J = 0$) and Gaussian beam show noise-like spatial spectra [Figs. 2(i)–2(k)]. Note that the effective spot diameters of both Gaussian and optical vortex beams were the same. Interestingly, the optical vortex enabled the reduction in fluence required for the single droplet ejection. In addition, it is worth mentioning that the circularly polarized Gaussian beam with SAM fabricated only non-uniform printed dot with many debris [Fig. 2(h)], manifesting that the close-packing effect inside the printed dots occurs by orbital angular momentum with the help of spin angular momentum.

The diameter of the printed dots formed when using optical vortices with $J = 2$ was found to be inversely proportional to the numerical aperture (NA) of the focusing optics. In this work, the minimum measured dot diameter was ~9 μm, which is less than a half of that (~20 μm) of dots typically printed using ink-jet printing technologies, at NA ~ 0.32 [Figs. 3(a) and 3(b)]. Direct print of dots with smaller diameters will be possible, but it will be impacted by a longitudinal electric field of tightly focused optical vortex beam with a high NA lens.[43] The minimum diameter of the printed dots will be expected to be ~5 μm at NA ~ 0.6.

By using optical vortex beams with $J = 2$, we were able to perform high-precision direct-printing of microdots with a positioning error of <7 μm, when using focusing optics with an NA below 0.3 [Figs. 3(a) and 3(c-1)–(c-4)]. Note that the positioning error was mostly limited by the positional accuracy (5 μm) of the piezo-actuators used in this work. It should be noted that the positional error of the dots formed using optical vortex beams with $J = 2$ was considerably lower (<45%) than the position error of dots formed using an optical vortex with $J = 0$ or a Gaussian beam that had a positional error of ~15.5 μm. This observation suggests that the TAM of the optical vortex beam acts to stabilize the flight of the droplets ejected from the jet. Such a straight flight of the ejected droplet will be originated from gyroscopic effects based on the TAM transfer. The two-dimensional patterns formed using a vortex beam with
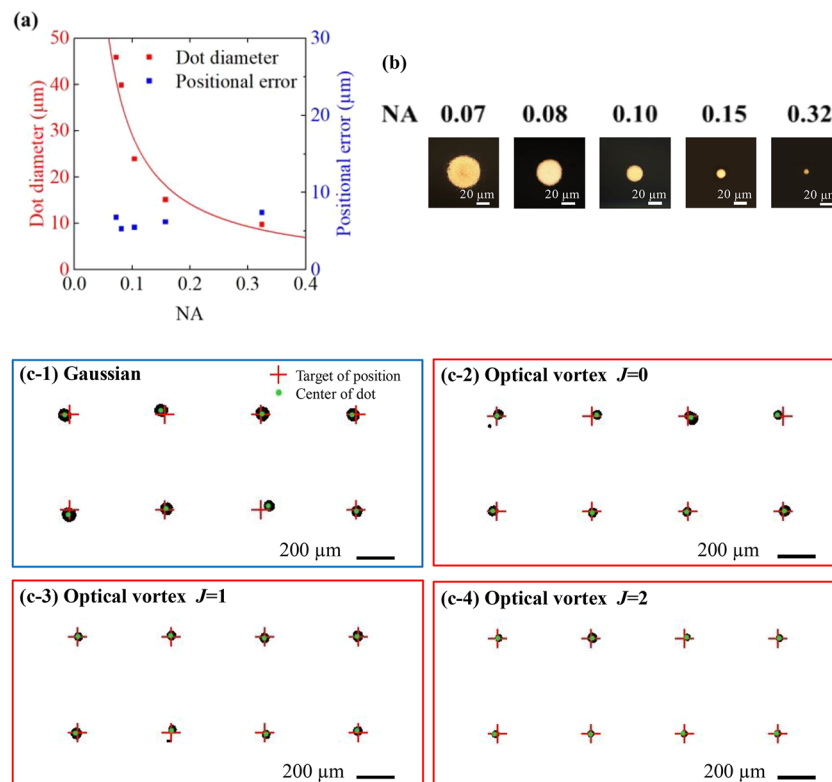
FIG. 3. (a) Diameter and positional error of the printed dots when using optics of different NA. The solid line indicates a fitting function of 3.0 (μm)/NA. (b) Optical images of the printed dots at various NA. Direct-print of two-dimensional dot arrays fabricated using (c-1) a Gaussian beam, (c-2) an optical vortex beam ($J = 0$), (c-3) an optical vortex beam ($J = 1$), and (c-4) an optical vortex beam ($J = 2$). "+" and "·" within the images indicate the target and printed positions of the dot, respectively.

FIG. 4. (a) "LIFT" comprised of gold microdots printed using OV-LIFT. (b) Dot array (with dot diameters ~15 μm) fabricated using OV-LIFT with NA ~ 0.15. (c) Dot array (with dot diameters ~9 μm) fabricated using OV-LIFT with NA ~ 0.3.

J = 2 are shown in Figs. 4(a)–4(c). Optical vortices with higher OAMs exhibit a rather large dark core, thus weakening the close-packing effect of the gold nanoparticles. Perfect vortices will allow for further improvement in the close-packing effects.

IV. DISCUSSION

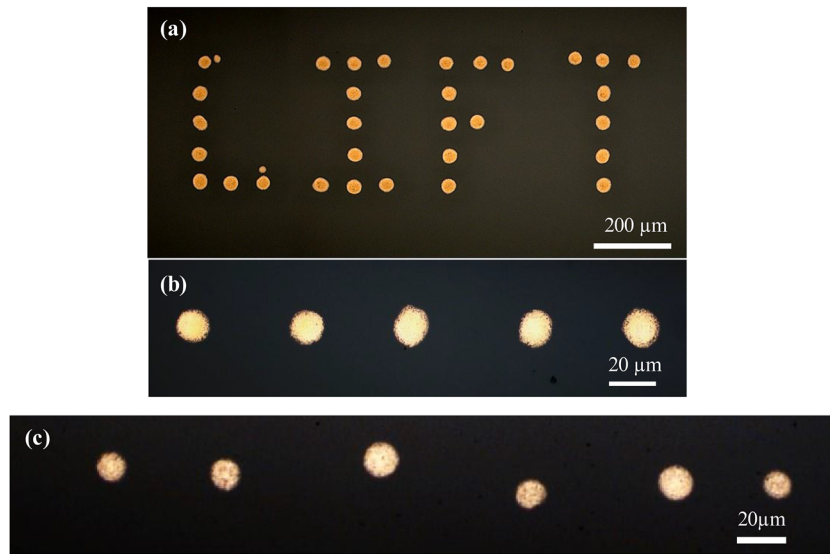In this work, optical vortex laser-induced breakdown within the donor material results in the formation of a cavitation bubble. The rapid collapse of the bubble forces the region of the donor material overlapping with the central dark core of the irradiating optical vortex to launch a high-speed jet of the donor material toward the receiver substrate. If we exclude the vaporization of the solution and the phase change of gold, we calculate that the irradiating optical vortex pulse will raise the temperature of the donor by ~400 K. This temperature rise is sufficient for the sintering of the gold nanoparticles.

The evolution of laser-induced cavitation bubbles is governed by the Rayleigh–Plesset equation,[44] which is expressed as follows:

$$\frac{P_B(t) - P_\infty(t)}{\rho_L} = R(t)\frac{d^2R(t)}{dt^2} + \frac{3}{2}\left(\frac{dR(t)}{dt}\right)^2 + \frac{4v_L}{R(t)}\frac{dR(t)}{dt} + \frac{2S}{\rho_L R(t)}, \tag{1}$$

where $P_B(t)$ and $P_\infty(t)$ are the pressures within the bubble and at an infinite distance outside the bubble, R(t) is the radius of the bubble, ρL ($\cong 1 \times 10^3$ kg/m^3) is the density of the liquid, vL (=1–3 $\times 10^{-4}$ m^2/s) is the dynamic viscosity, and S ($\cong$50 mN m) is the surface tension. Assuming that the spatial form of the blister, which forms in the irradiated region of the donor film, reflects the shape of the cavitation bubble, we modeled the temporal evolution of the

bubble by fitting to the shape of the blister with a semi-spherical function [Figs. 5(a) and 5(b)]. The shrinkage of the optical vortex induced cavitation bubble occurs rapidly within ~3 μs after the laser pulse irradiation, whereas the Gaussian beam induced cavitation bubble is still growing. By utilizing the experimental temporal evolution function of the bubble evaluated by fitting measured bubble diameters with a third-order polynomial function, we determined that the optical vortex produces a negative cavitation pressure PB at
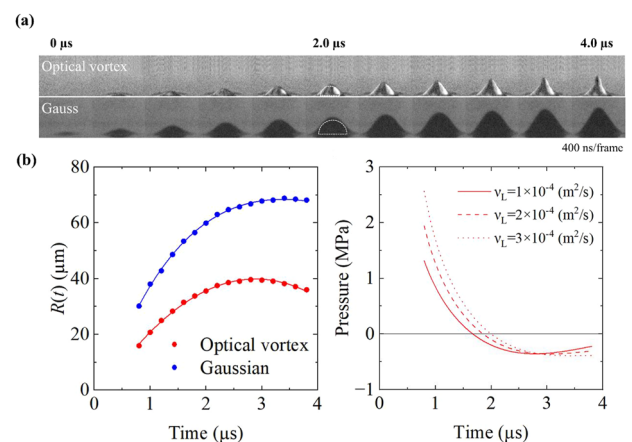
FIG. 5. (a) Time-lapse of the evolution of the blister formation in a time period of 0–4 μs after the illumination of optical vortex and Gaussian pulses. The blister outlines (the dashed line on the optical image at 2 μs) are fitted by a semi-circle to estimate the cavitation bubble radius. (b) Temporal evolution of the cavitation bubble radius produced by illumination by both optical vortex and Gaussian pulses. (c) Plot of the estimated cavitation pressure outside (positive) and inside (negative) the bubble based on the Rayleigh–Plesset equation.

$t \sim 2\ \mu s$ in the donor film (the negative/inward cavitation pressure reached -0.5 MPa at $t = 2$–$4\ \mu s$) via the cavitation bubble shrinkage (the jet formation then occurs), which forces the nanoparticles to coalesce within the bubble, resulting in close packing of the gold particles [Fig. 5(c)].[45] In contrast, illumination with a Gaussian beam does not result in close packing of nanoparticles mostly due to its positive/outward cavitation pressure effect associated with relatively slow shrinkage of the cavitation bubble. These theoretical results support our experimental observations.

Other contributors to the formation of close-packed gold nanoparticles may be thermo-fluid dynamic processes, such as the Marangoni effects associated with the ring-shaped spatial form of the irradiating optical vortex beam. The optical vortex induced Marangoni force acts to push the laser heated region of the donor film toward the non-heated region via surface tension gradients. This has also been shown to result in the collection of gold nanoparticles within the region of donor films overlapped with the dark central region of an irradiating vortex beam.[46]

Numerical analysis of the laser-induced fluid dynamics, including Marangoni convection,[47,48] was performed using commercial software (COMSOL Multiphysics®). We assumed cylindrical symmetry along the laser beam propagation direction (optical axis) and that plasmonic heating of the gold nanoparticles was a heat source. The laser-induced temperature gradient in the donor film was simulated using the conventional heat diffusion equation and the Navier–Stokes equation under the Boussinesq approximation.[49] The density ρ, the specific heat capacity C_p, the absorption cross section σ_{abs}, and the thermal conductivity k of the donor were then assumed to be 1.1×10^3 kg/m³, 2.2 kJ/(kg K), 2.5×10^{-25} m⁻², and 0.25 W/(m K), respectively. To simplify the numerical modeling, the latent heat of evaporation was excluded. The Marangoni pressure was estimated to be at the highest $\sim$0.03 MPa and was considered negligible in comparison with the cavitation pressure. The repulsive optical force under illumination by the optical vortex could confine the nanoparticles within the region of the central dark spot; however, its contribution was numerically calculated to be $\sim$0.001 MPa and was also considered negligible in comparison with the cavitation pressure (this calculation was performed via surface integration of Maxwell's stress tensor[50,51]).

The orbital angular momentum of the irradiating vortex beam forces the donor film to twist via plasmonic absorption by the gold nanoparticles.[52] This results in spinning/twisting motion of the generated donor jet, which is terminated by Stokes drag torque.[53] The terminal rotation frequency (f) of the jet can be calculated using the following equation:

$$f \approx \frac{1}{8\pi^2 \sigma a^2 L} \frac{E}{\omega} \frac{J}{\Delta t}, \qquad (2)$$

where σ is the viscosity of the surrounding air, a and L are the radius and height of the jet, respectively, E is the pulse energy, ω and J are the angular frequency and TAM of the irradiating optical vortex, respectively, and Δt is the pulse duration. Using this equation and the experimental parameters in this work, the calculated terminal rotation frequency was 1.1×10^2 kilo-rotations/s (krps).

The experimental rotation frequency of the donor material jet was directly observed using an ultrahigh speed camera [Fig. 6(a), Multimedia view]. It was found to be linearly proportional to the irradiating optical vortex pulse energy. It should be noted that an
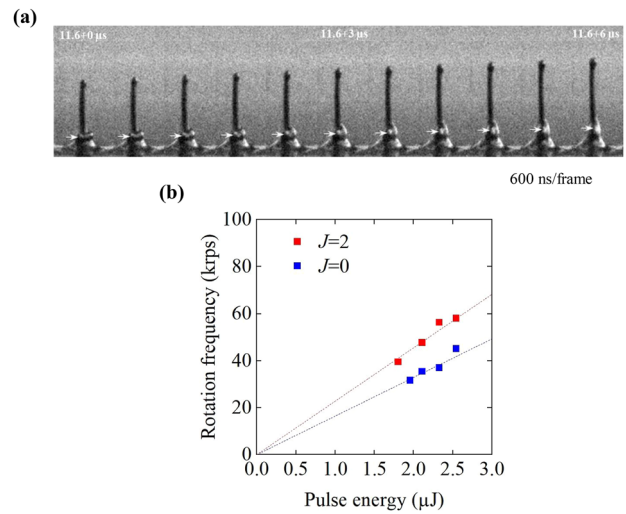

FIG. 6. (a) Time-lapse of the evolution of the droplet ejection in a time period of 11.6–18.2 μs after the illumination of the optical vortex pulse. The blister and ejected jet were twisted in the clockwise direction. Temporal evolution of this "twist" is visualized by the white arrows overlaid on the images (Multimedia available online). (b) Plot of the rotational speeds of the blister as a function of the pulse energy of the irradiating optical vortex with $J = 2$ and 0. The rotation frequency of the blister was found to be linearly proportional to the irradiating laser pulse energy. Multimedia available online.

optical vortex with non-zero ℓ and zero TAM ($J = 0$) exhibits a non-zero azimuthal linear momentum under the paraxial approximation, and this results in the spinning motion of the jet. The plots showing the rotational frequency as a function of pulse energy for beams with $J = 2$ and $J = 0$ are shown in Fig. 6(b). The highest experimentally observed rotation frequency was $\sim$6 × 10 krps, which was approximately a half the theoretically calculated value. We believe that this discrepancy can be attributed to the dissipation of OAM via fluid dynamic processes, such as cavitation bubbling and Marangoni convection. The ultrafast spinning motion of the jet reinforces the close-packing of the gold nanoparticles within the dark core so as to further improve the electrical conductivity of the printed dots.

V. CONCLUSION

We have observed and investigated optical vortex-facilitated, two-dimensional direct-printing of sintered metallic microdots with a diameter of less than 20 μm (the minimum printed dot diameter is measured to be 9 μm) beyond the limitation of conventional nozzle-based ink-jet printing. Here, the OAM of an irradiating optical vortex forces the close-packing and sintering of gold nanoparticles, and it significantly improves the positional accuracy of the printed dots, with the assistance of SAM. Our experimental observations are supported by theoretical models that consider a number of processes by which the optical fields interact with the irradiated materials. We believe that there is scope to further improve the accuracy of the theoretical model through further consideration of the hydrodynamic interaction that occurs between the irradiating light field and the donor material.

AUTHOR DECLARATIONS

Conflict of Interest

The authors have no conflicts to disclose.

Author Contributions

R.W. and H.K. contributed equally to this work.

Rong Wei: Data curation (lead); Formal analysis (equal); Investigation (equal); Software (supporting); Visualization (equal); Writing – original draft (equal); Writing – review & editing (equal). **Haruki Kawaguchi**: Data curation (lead); Formal analysis (lead); Investigation (equal); Software (lead); Validation (equal); Visualization (equal); Writing – original draft (equal); Writing – review & editing (equal). **Kaito Sato**: Data curation (equal); Software (equal); Visualization (equal). **Sayaka Kai**: Data curation (equal); Software (equal); Visualization (equal). **Keisaku Yamane**: Data curation (supporting); Investigation (supporting); Visualization (equal); Writing – review & editing (equal). **Ryuji Morita**: Conceptualization (supporting); Formal analysis (supporting); Methodology (supporting); Writing – review & editing (equal). **Ken-ichi Yuyama**: Formal analysis (equal); Investigation (supporting); Project administration (equal); Software (equal); Writing – review & editing (supporting). **Satoyuki Kawano**: Formal analysis (equal); Software (equal); Writing – review & editing (supporting). **Katsuhiko Miyamoto**: Data curation (supporting); Investigation (equal); Software (supporting); Validation (equal); Visualization (supporting); Writing – review & editing (equal). **Nobuyuki Aoki**: Data curation (equal); Formal analysis (supporting); Investigation (equal); Validation (supporting); Writing – review & editing (supporting). **Takashige Omatsu**: Conceptualization (equal); Formal analysis (equal); Funding acquisition (equal); Investigation (equal); Methodology (equal); Project administration (equal); Supervision (equal); Validation (equal); Writing – original draft (equal); Writing – review & editing (equal).

DATA AVAILABILITY

The data that support the findings of this study are available from the corresponding author upon reasonable request.

REFERENCES

[1]M. Singh, H. M. Haverinen, P. Dhagat, and G. E. Jabbour, "Inkjet printing—Process and its applications," Adv. Mater. **22**(6), 673–685 (2010).

[2]C. Vieu, F. Carcenac, A. Pépin, Y. Chen, M. Mejias, A. Lebib, L. Manin-Ferlazzo, L. Couraud, and H. Launois, "Electron beam lithography: Resolution limits and applications," Appl. Surf. Sci. **164**(1–4), 111–117 (2000).

[3]S. Vignolini, N. A. Yufa, P. S. Cunha, S. Guldin, I. Rushkin, M. Stefik, K. Hur, U. Wiesner, J. J. Baumberg, and U. Steiner, "A 3D optical metamaterial made by self-assembly," Adv. Mater. **24**(10), OP23–OP27 (2012).

[4]S. Friedensen, J. T. Mlack, and M. Drndić, "Materials analysis and focused ion beam nanofabrication of topological insulator Bi$_2$Se$_3$," Sci. Rep. **7**(1), 13466 (2017).

[5]O. Song, D. Rhee, J. Kim, Y. Jeon, V. Mazánek, A. Söll, Y. A. Kwon, J. H. Cho, Y.-H. Kim, Z. Sofer, and J. Kang, "All inkjet-printed electronics based on electrochemically exfoliated two-dimensional metal, semiconductor, and dielectric," npj 2D Mater. Appl. **6**(1), 64 (2022).

[6]A. Kamyshny and S. Magdassi, "Conductive nanomaterials for printed electronics," Small **10**(17), 3515–3535 (2014).

[7]V. Beedasy and P. J. Smith, "Printed electronics as prepared by inkjet printing," Materials **13**(3), 704 (2020).

[8]Y. Khan, A. Thielens, S. Muin, J. Ting, C. Baumbauer, and A. C. Arias, "A new frontier of printed electronics: Flexible hybrid electronics," Adv. Mater. **32**(15), 1905279 (2020).

[9]G. Hu, T. Albrow-Owen, X. Jin, A. Ali, Y. Hu, R. C. T. Howe, K. Shehzad, Z. Yang, X. Zhu, R. I. Woodward, T.-C. Wu, H. Jussila, J.-B. Wu, P. Peng, P.-H. Tan, Z. Sun, E. J. R. Kelleher, M. Zhang, Y. Xu, and T. Hasan, "Black phosphorus ink formulation for inkjet printing of optoelectronics and photonics," Nat. Commun. **8**(1), 278 (2017).

[10]M. Kuang, J. Wang, B. Bao, F. Li, L. Wang, L. Jiang, and Y. Song, "Inkjet printing patterned photonic crystal domes for wide viewing-angle displays by controlling the sliding three phase contact line," Adv. Opt. Mater. **2**(1), 34–38 (2014).

[11]M. Théry, "Micropatterning as a tool to decipher cell morphogenesis and functions," J. Cell Sci. **123**(24), 4201–4213 (2010).

[12]A. Doraiswamy, T. M. Dunaway, J. J. Wilker, and R. J. Narayan, "Inkjet printing of bioadhesives," J. Biomed. Mater. Res., Part B **89B**(1), 28–35 (2009).

[13]D. Lohse, "Fundamental fluid dynamics challenges in inkjet printing," Annu. Rev. Fluid Mech. **54**, 349–382 (2022).

[14]A. Lee, K. Sudau, K. H. Ahn, S. J. Lee, and N. Willenbacher, "Optimization of experimental parameters to suppress nozzle clogging in inkjet printing," Ind. Eng. Chem. Res. **51**(40), 13195–13204 (2012).

[15]J. Bohandy, B. F. Kim, and F. J. Adrian, "Metal deposition from a supported metal film using an excimer laser," J. Appl. Phys. **60**(4), 1538–1539 (1986).

[16]M. Colina, M. Duocastella, J. M. Fernández-Pradas, P. Serra, and J. L. Morenza, "Laser-induced forward transfer of liquids: Study of the droplet ejection process," J. Appl. Phys. **99**, 084909 (2006).

[17]J. M. Fernández-Pradas, P. Sopeña, S. González-Torres, J. Arrese, A. Cirera, and P. Serra, "Laser-induced forward transfer for printed electronics applications," Appl. Phys. A **124**(2), 214 (2018).

[18]P. Sopeña, J. Sieiro, J. M. Fernández-Pradas, J. M. López-Villegas, and P. Serra, "Laser-induced forward transfer: A digital approach for printing devices on regular paper," Adv. Mater. Technol. **5**(6), 2000080 (2020).

[19]R. Pohl, C. W. Visser, G.-W. Römer, D. Lohse, C. Sun, and B. Huis in 't Veld, "Ejection regimes in picosecond laser-induced forward transfer of metals," Phys. Rev. Appl. **3**(2), 024001 (2015).

[20]M. Kandyla, S. Chatzandroulis, and I. Zergioti, "Laser induced forward transfer of conducting polymers," Opto-Electron. Rev. **18**(4), 345–351 (2010).

[21]M. Colina, P. Serra, J. M. Fernández-Pradas, L. Sevilla, and J. L. Morenza, "DNA deposition through laser induced forward transfer," Biosens. Bioelectron. **20**(8), 1638–1642 (2005).

[22]C. F. Brasz, C. B. Arnold, H. A. Stone, and J. R. Lister, "Early-time free-surface flow driven by a deforming boundary," J. Fluid Mech. **767**, 811–841 (2015).

[23]S. A. Mathews, R. C. Y. Auyeung, H. Kim, N. A. Charipar, and A. Piqué, "High-speed video study of laser-induced forward transfer of silver nano-suspensions," J. Appl. Phys. **114**(6), 64910 (2013).

[24]C. Boutopoulos, I. Kalpyris, E. Serpetzoglou, and I. Zergioti, "Laser-induced forward transfer of silver nanoparticle ink: Time-resolved imaging of the jetting dynamics and correlation with the printing quality," Microfluid. Nanofluid. **16**(3), 493–500 (2014).

[25]J. Mikšys, G. Arutinov, and G. R. B. E. Römer, "Pico- to nanosecond pulsed laser-induced forward transfer (LIFT) of silver nanoparticle inks: A comparative study," Appl. Phys. A **125**(12), 814 (2019).

[26]L. Allen, M. W. Beijersbergen, R. J. C. Spreeuw, and J. P. Woerdman, "Orbital angular momentum of light and the transformation of Laguerre-Gaussian laser modes," Phys. Rev. A **45**(11), 8185–8189 (1992).

[27]G. Molina-Terriza, J. P. Torres, and L. Torner, "Twisted photons," Nat. Phys. **3**(5), 305–310 (2007).

[28]M. Dienerowitz, M. Mazilu, P. J. Reece, T. F. Krauss, and K. Dholakia, "Optical vortex trap for resonant confinement of metal nanoparticles," Opt. Express **16**(7), 4991 (2008).

[29]N. Bozinovic, Y. Yue, Y. Ren, M. Tur, P. Kristensen, H. Huang, A. E. Willner, and S. Ramachandran, "Terabit-scale orbital angular momentum mode division multiplexing in fibers," Science **340**(6140), 1545–1548 (2013).

[30]S. Ramachandran and P. Kristensen, "Optical vortices in fiber," Nanophotonics **2**(5–6), 455–474 (2013).

[31]A. Mair, A. Vaziri, G. Weihs, and A. Zeilinger, "Entanglement of the orbital angular momentum states of photons," Nature **412**(6844), 313–316 (2001).

[32]M. Kamper, H. Ta, N. A. Jensen, S. W. Hell, and S. Jakobs, "Near-infrared STED nanoscopy with an engineered bacterial phytochrome," Nat. Commun. **9**(1), 4762 (2018).

[33]K. A. Forbes and G. A. Jones, "Optical vortex dichroism in chiral particles," Phys. Rev. A **103**(5), 053515 (2021).

[34]D. L. Andrews, "Quantum formulation for nanoscale optical and material chirality: Symmetry issues, space and time parity, and observables," J. Opt. **20**, 033003 (2018).

[35]K. Toyoda, K. Miyamoto, N. Aoki, R. Morita, and T. Omatsu, "Using optical vortex to control the chirality of twisted metal nanostructures," Nano Lett. **12**(7), 3645–3649 (2012).

[36]A. Ablez, K. Toyoda, K. Miyamoto, and T. Omatsu, "Nanotwist of aluminum with irradiation of a single optical vortex pulse," OSA Continuum **4**(2), 403–408 (2021).

[37]F. Takahashi, K. Miyamoto, H. Hidai, K. Yamane, R. Morita, and T. Omatsu, "Picosecond optical vortex pulse illumination forms a monocrystalline silicon needle," Sci. Rep. **6**(2015) , 21738 (2016).

[38]J. Lee, Y. Arita, S. Toyoshima, K. Miyamoto, P. Panagiotopoulos, E. M. Wright, K. Dholakia, and T. Omatsu, "Photopolymerization with light fields possessing orbital angular momentum: Generation of helical microfibers," ACS Photonics **5**(10), 4156–4163 (2018).

[39]Y. Arita, J. Lee, H. Kawaguchi, R. Matsuo, K. Miyamoto, K. Dholakia, and T. Omatsu, "Photopolymerization with high-order Bessel light beams," Opt. Lett. **45**(14), 4080–4083 (2020).

[40]K. Y. Bliokh, F. J. Rodríguez-Fortuño, F. Nori, and A. V. Zayats, "Spin-orbit interactions of light," Nat. Photonics **9**(12), 796–808 (2015).

[41]R. Nakamura, H. Kawaguchi, M. Iwata, A. Kaneko, R. Nagura, S. Kawano, K. Toyoda, K. Miyamoto, and T. Omatsu, "Optical vortex-induced forward mass transfer: Manifestation of helical trajectory of optical vortex," Opt. Express **27**(26), 38019–38027 (2019).

[42]H. Kawaguchi, K. Umesato, K. Takahashi, K. Yamane, R. Morita, K. Yuyama, S. Kawano, K. Miyamoto, M. Kohri, and T. Omatsu, "Generation of hexagonal close-packed ring-shaped structures using an optical vortex," Nanophotonics **11**(4), 855–864 (2022).

[43]Y. Zhao, J. S. Edgar, G. D. M. Jeffries, D. McGloin, and D. T. Chiu, "Spin-to-Orbital angular momentum conversion in a strongly focused optical beam," Phys. Rev. Lett. **99**(7), 073901 (2007).

[44]M. S. Plesset and A. Prosperetti, "Bubble dynamics and cavitation," Annu. Rev. Fluid Mech. **9**(1), 145–185 (1977).

[45]K. Yuyama, H. Kawaguchi, R. Wei, and T. Omatsu, "Fabrication of an array of hemispherical microlasers using optical vortex laser-induced forward transfer," ACS Photonics **10**, 4045 (2023).

[46]M. Tamura, T. Omatsu, and T. Iida, "Nanoneedle formation via dough-nut beam-induced Marangoni effects," Opt. Express **30**(20), 35136–35145 (2022).

[47]B. W. Li, M. C. Zhong, and F. Ji, "Laser induced aggregation of light absorbing particles by Marangoni convection," Appl. Sci. **10**(21), 7795 (2020).

[48]K. Gupta, K. M. Kolwankar, B. Gore, J. A. Dharmadhikari, and A. K. Dharmadhikari, "Laser-driven Marangoni flow and vortex formation in a liquid droplet," Phys. Fluids **32**(12), 121701 (2020).

[49]E. A. Spiegel and G. Veronis, "On the Boussinesq approximation for a compressible fluid," Astrophys. J. **131**, 442 (1960).

[50]O. M. Maragò, P. H. Jones, P. G. Gucciardi, G. Volpe, and A. C. Ferrari, "Optical trapping and manipulation of nanostructures," Nat. Nanotechnol. **8**(11), 807–819 (2013).

[51]A. Lehmuskero, P. Johansson, H. Rubinsztein-Dunlop, L. Tong, and M. Käll, "Laser trapping of colloidal metal nanoparticles," ACS Nano **9**(4), 3453–3469 (2015).

[52]M. E. J. Friese, J. Enger, H. Rubinsztein-Dunlop, and N. R. Heckenberg, "Optical angular-momentum transfer to trapped absorbing particles," Phys. Rev. A **54**(2), 1593–1596 (1996).

[53]P. R. N. Childs, *Rotating Flow*, 1st ed. (Elsevier, New York, NY, 2010).

20 April 2024 13:25:05